

Catalysis Science & Technology

Accepted Manuscript



This is an *Accepted Manuscript*, which has been through the Royal Society of Chemistry peer review process and has been accepted for publication.

Accepted Manuscripts are published online shortly after acceptance, before technical editing, formatting and proof reading. Using this free service, authors can make their results available to the community, in citable form, before we publish the edited article. We will replace this *Accepted Manuscript* with the edited and formatted *Advance Article* as soon as it is available.

You can find more information about *Accepted Manuscripts* in the [Information for Authors](#).

Please note that technical editing may introduce minor changes to the text and/or graphics, which may alter content. The journal's standard [Terms & Conditions](#) and the [Ethical guidelines](#) still apply. In no event shall the Royal Society of Chemistry be held responsible for any errors or omissions in this *Accepted Manuscript* or any consequences arising from the use of any information it contains.

ARTICLE

Monodispersed Pt atoms Anchored on N-doped Graphene as Efficient Catalysts for CO Oxidation: A First-principles Investigation†

Cite this: DOI: 10.1039/x0xx00000x

Xin Liu,^a Yanhui Sui,^a Ting Duan,^a Changgong Meng^a and Yu Han^b

Received 00th January 2014,

Accepted 00th January 2014

DOI: 10.1039/x0xx00000x

www.rsc.org/

We performed first-principles based calculations to investigate the electronic structure and the potential catalytic performance of Pt atoms monodispersed on N-doped graphene in CO oxidation. We showed that N-doping can introduce localized defect states to the vicinal of the Fermi level of graphene which will effectively stabilize the deposited Pt atoms. The binding of a single Pt atom onto a stable cluster of 3 pyridinic N (PtN3) is up to -4.47 eV, making the diffusion and aggregation of anchored Pt atoms hard to take place. Both the reaction thermodynamics and kinetics suggest that CO oxidation over PtN3 would proceed through the Langmuir–Hinshelwood mechanism. The reaction barriers for the formation and dissociation of peroxide-like intermediate are determined as low as 0.01 and 0.08 eV, respectively, while that for the regeneration is only 0.15 eV, proving the potential high catalytic performance of PtN3 in CO oxidation, especially at low temperatures. The Pt-d states that are up-shifted by the Pt-N interaction, accounts for the enhanced activation of O₂ and the efficient formation and dissociation of the peroxide-like intermediate.

1. Introduction

For decades, converting environmental-harmful pollutants, including CO, to eco-benign CO₂ and H₂O, for the purpose of emission control from combustion, industrial chemical processes and etc, has attracted considerable attention. Though transition metal (TM) based catalysts, including Pt¹⁻³, Pd,^{4,5} Rh⁶⁻⁸, Au⁹⁻¹¹ and etc, can catalyze CO oxidation effectively, they are expensive and usually require to work at high temperatures to achieve a reasonable performance due to their stronger affinity to CO.¹² Scientists have been working continuously to develop novel catalysts for low temperature CO oxidation.¹³⁻¹⁵

Finely dispersed TM nanoparticles (NPs), which exhibit distinctly different catalytic performance such as the high activity and selectivity and superior stability as compared with the corresponding bulk materials, are efficient heterogeneous catalysts for several important chemical processes, such as CO oxidation.¹⁶⁻¹⁹ Even in these cases, the mass-averaged catalytic efficiency of TM is still low as compared with those of the homogeneous counterparts, because merely the surface sites are catalytic active and they contribute only a small percentage to the total usage of TM. Given the high price and limited resources of TMs, improving the mass-averaged catalytic efficiency in heterogeneous TM-based catalysts while keeping

or even prompting the catalytic performance is of great significance and highly desired.²⁰ The reactivity of TM NPs are determined by their localized d states,²¹ therefore, low-coordination and unsaturated atoms are the reaction sites over TM NPs.²² This is completely different from NPs of sp metals, where the free-electron like behavior of sp electrons makes the quantum size effect crucial.^{23, 24} To this end, downsizing the TM NPs to small clusters or single atoms that are catalytic active would be a feasible way to achieve a higher density of active sites for catalytic reactions and to improve the mass-averaged catalytic performance of TMs.²⁰

As the size of TM NPs goes down, the impact of NP-support interfacial interaction would become more apparent. Depending on the interfacial structure,²⁵⁻²⁷ the bonding between TM atoms and the support,²⁷⁻²⁹ this interaction would introduce strains at the interface, cause the energy and spacial redistribution of the TM states and thus change the performance of the resulting catalysts.^{30, 31} The interfacial interaction may also help to effectively stabilize the tiny TM NPs or atoms and prohibit them from sintering under realistic reaction conditions, which are the key challenges for implementation of monodispersed ultrafine TM catalysts for practical applications.^{32, 33} In this sense, a careful screening of the metal-support interactions would be necessary to rationalize the design of mono-dispersed ultrafine TM NPs or single TM atoms as efficient catalyst for a specific reaction. Combining

^a School of Chemistry, Dalian University of Technology, Dalian, China; E-mail: xliu@dlut.edu.cn. ^b Advanced Membranes and Porous Materials Center, Physical Sciences and Engineering Division, King Abdullah University of Science and Technology, Thuwal 23955-6900, Saudi Arabia.

the highly active monodispersed TM atoms and suitable support materials, several single-atom catalysts have been found efficient for CO oxidation, such as Pt/FeO_x,¹⁵ Pt/Al₂O₃,¹⁸ Au/FeO_x,³⁴ Pd/CeO₂,³⁵ Ir/Fe(OH)_x,¹⁴ Ag/MnO_x,³⁶ Pt/Graphene³⁷ and etc, and the superior catalytic performance was explained with the high reactivity of the partially occupied d states that was shifted to the Fermi level (E_F) by the TM-support interaction.

The large surface area, excellent conductivity, outstanding mechanical strength and potential low cost for large scale production make graphene (GN), the only 2D member in the family of allotropes of carbon, a superior support material for dispersion of TM catalysts.³⁸ Among various methods for functionalization, substitutional doping has been proved to be an effective way to modulate properties of GN.³⁹ The N-doped graphene(NG) not only inherits the outstanding properties of GN as a catalyst support, but also demonstrates some superior properties for catalytic and electronic applications, as the introduction of N alters the spatial and energy distribution of electronic states and dramatically changes the local reactivity.⁴⁰ NG has been used for several important reactions, such as oxygen reduction in fuel cell, hydrogen evolution in catalytic reduction of water, and etc.^{39, 41} Among various N-doping species, the pyridinic and quaternary N account for the high ORR activity of NG and their population in NG can be controlled by the fabrication methods.^{39, 42, 43} The pyridinic N has also been identified as the anchoring point for TM atoms and NPs and is responsible for the superior electrocatalytic performance of well dispersed Pt atoms and small Pt clusters in Pt/NG composites as compared with Pt/GN due to the modified interfacial interaction by N-doping.⁴⁴⁻⁴⁷ TM atoms stabilized by defects on GN have been proposed to be efficient for CO oxidation previously.⁴⁸⁻⁵¹ However, the contribution of N-doping on the stability and catalytic performance of the TM atoms and NPs dispersed on NG are rarely explored.

Inspired by previous works and to develop principles for a rational design of single-atom catalysts for low temperature CO oxidation, we investigated the electronic structure and potential catalytic performance of Pt atoms dispersed on NG in CO oxidation by first-principles-based calculations. We focused on the impact of N-doping on the interfacial interactions and the catalytic activity of these mono-dispersed Pt atoms. Based on the calculated thermodynamics and kinetics data, we showed that CO oxidation would proceed through the Langmuir–Hinshelwood mechanism. The reaction energy barriers for the formation and dissociation of peroxide-like intermediate are as low as 0.01 and 0.08 eV, respectively, while that for the regeneration of the dispersed Pt atom is only 0.15 eV. The localized Pt-d states that are up-shifted to the E_F by the interfacial interaction play a superior role in enhancing the activation of O₂ and turning the formation and dissociation of peroxide-like intermediate more efficient. The rest of the manuscript was organized as the following, the information on model setup and theoretical methods was described in Section 2, the results were presented and discussed in Section 3 and concluded in Section 4.

2. Theoretical methods

The electronic structure calculations were performed using a first-principles-based approach, with DFT semicore pseudopotentials in conjunction with double numerical basis sets including d-polarization functions as implemented in the DMol³ package.⁵² The exchange and correlation functional of Perdew, Burke and Ernzerhof (PBE) within the generalized gradient approximation (GGA) was used for structure relaxations, location of transition states (TSs) and subsequent analysis.⁵³⁻⁵⁵ The structure relaxations were performed in a 2-step way to lower the computational cost. The NG supports and the Pt/NG composites were preoptimized with empirical potentials derived from first-principles-based calculations^{56, 57} and were then further relaxed within the aforementioned ab-initio scheme to reduce the residue forces to below 1×10^{-2} eV/Å. The TSs were located with the synchronous method with conjugated gradient refinements.⁵⁸ The real-space global orbital cutoff radius was set as 4.6 Å and the convergence criterion on total energy in all self-consistent field calculations was set to 2×10^{-4} eV to ensure the quality of results. With the above setup, the bulk lattice parameter of face-center-cubic Pt is reproduced as $a = 3.98$ Å, while the minimum C-C distance in pristine GN is 1.42 Å.

The electronic structures of NG and the Pt atom deposited on NG were investigated with a hexagonal 4×4 supercell of pristine GN. The vacuum layer was set to be larger than 20 Å to avoid the interactions among mirror images. Monkhorst-Pack k-point scheme was adapted to sample the Brillouin zone. We used a Γ centered $4 \times 4 \times 1$ k-point grid during the structure relaxations and the search for the TSs, while a $20 \times 20 \times 1$ k-point grid to explore the electronic properties.⁵⁹ The Hirshfeld scheme was employed to estimate the amount of charge transfer at interface and upon adsorption.⁶⁰ Test calculations were performed on a 162-atom supercell (9×9 supercell of GN) and all gave essentially the same results.

The binding energy (E_b) of Pt atom onto NG was calculated as the difference in total energy between the Pt atomically deposited NG (PtNG) and the clean NG plus the freestanding Pt atom, following Equation (1).

$$E_b = E_{PtNG} - (E_{Pt} + E_{NG}) \quad (1)$$

The formation energy (E_f) of all NG and PtNG structures was calculated with respect to stoichiometry (n_x) of elements ($x=C, N$ and Pt) and their chemical potentials (μ_x) which were derived from bulk diamond, gaseous N₂ and bulk face-center-cubic Pt, according to Equation (2)

$$E_f = E_{total} - \sum_x n_x \mu_x \quad (2)$$

The adsorption energy (E_{ad}) of reaction species, such as CO, O₂, O and CO₂, is calculated as the difference in total energy between the PtNG with adsorbate and clean PtNG plus the adsorbate in gas phase, following Equation (3).

$$E_{ad} = E_{adsorbate+PtNG} - (E_{PtNG} + E_{adsorbate}) \quad (3)$$

3. Results and discussions

3.1 Pt atomic deposition on N-doped graphene

Depending on the doping methods used, there are three commonly observed N-doped structures in NG, namely the pyridinic N, the pyrrolic N and the graphite N.^{61,62} Due to the difference in bonding of these N species with surrounding atoms, the stability of formed N-doped structures is dramatically different. We calculated the formation energy (E_f) of several N-doped structures according to Eq(2). The E_f of pristine GN is -13.24 eV. The formation of a vacant defect on pristine GN (Fig. 1, C3) requires an energy input of 7.69 eV, but is still thermodynamically permitted.²⁵ In this structure, 2 of the 3 C atoms around the vacancy will bond together with the dangling bonds localized on the remaining C atom. The existence of pyridinic N requires formation of edge or vacant defects. Doping the C atom associated with the dangling bonds in C3 with a N atom (Fig. 1, N1) will form a pyridinic N and the structure is stabilized by 2.08 eV. Subsequent doping of another C atom that newly bonded together with another N atom can further stabilize the defect by only 0.34 eV (Fig. 1, N2). As new dangling bonds are introduced, the contribution of N doping to the stability at this step is not as significant as the introduction of first pyridinic N. When all the 3 C atoms around the vacancy are substituted by N (Fig. 1, N3), the E_f goes down to -9.27 eV as the dangling bonds due to formation of vacancy are completely vanished. The formation of pyrrolic N as a competing process for formation of N1 was also considered, but was found less stable by 2.91 eV as compared with N1. As for the case of graphitic N, the corresponding E_f goes up by 0.98 eV with respect to that of pristine GN, implying that the introduction of graphitic N will only give rise to moderate reactivity. The E_s of these NG structures are all negative implying that the exothermic nature of their formation. According to the calculated E_f of these N-doped structures, the graphitic N is the most stable N-doped structure in NG though the formation process may be hindered kinetically. The formation of pyrrolic N is thermodynamically less preferred as compared with pyridinic N. The relative stability of NG structures depends strongly on how the dangling bonds and defects states are passivated by introduction of N atoms. These findings are also supported by the experimental finding that the graphite N is the dominant N-doped structures after annealing of NG at high temperatures (>700 K) while pyridinic N is the majority N-doped structure when NG is annealed at moderate temperatures (~ 500 K) and is more stable as compared with pyrrolic N.⁶¹

Experimentally, doping GN with desired N-doped structures has been successfully realized by altering the reaction condition or the precursors.⁶¹ As the synthesis of NG with solely pyridinic N has been realized⁶³ and pyridinic N-doped NG has been used as catalyst support to anchor TM atoms, we focused on NG doped with pyridinic N.⁴⁵ To verify the possible existence of these NG structures, the corresponding core level shifts of N-1s state were calculated. Taking the N-1s level of

gas-phase N_2H_4 as a reference, the calculated N-1s core level shifts of N1, N2 and N3 fall in the range from 0.05 eV to 0.10 eV, which compare well with the experimental XPS results, proving the dominant population of these structures in as synthesized NG.⁶⁴

The electronic structure of these NG structures was examined by DOS analysis (Fig. 1, right panel). It is apparent that there are sharp spikes within 0.5 eV from the E_F on the DOS curves of all these NG structures and the DOS intensity around E_F is significantly altered after the introduction of pyridinic N. For the case of N3, a N-2p state is shifted to standing right at the E_F . The charge densities of these states were extracted (Fig. 1, left panel) which further prove that these spikes correspond to the dangling bonds localized on N and adjacent C atoms. As the DOS intensity at E_F has been recognized as a good indicator for the reactivity of sp-electronic system,²³ these NG structures are expected to exhibit superior reactivity to anchor TM atoms and NPs. Vacancy and doping defects like these have also been predicted to alter the electronic properties of GN and modulate its chemical reactivity toward adsorbates.⁶⁵⁻⁶⁷ We recently investigated the ability of various defects on graphene on anchoring TM atoms and found that the electronic structure of the deposited TM atoms and clusters correlated strongly with the interfacial interaction.²⁵ We expect these NG structures, especially N3, would act as anchoring points to bind strongly with the Pt atoms and the interfacial Pt-N interactions will further tune the electronic structure of dispersed Pt atoms to demonstrate unusual reactivity.

As there is an energy barrier for breaking of the C-C bond in N1 and N2 is too reactive to survive in the solution-based deposition route, the formation of PtN1 and PtN2 would be dependent strongly on the synthesis condition. In N3, all the number of dangling bonds is minimized, which guarantees not only its survival during liquid phase processing but also the trapping of Pt atoms. Therefore, we will focus on N3 in the subsequent discussion.

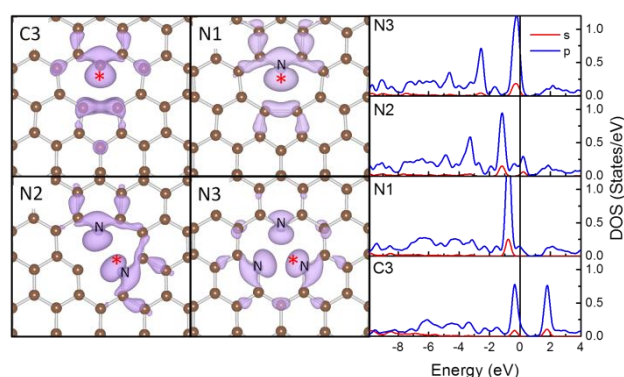


Fig. 1 Structures (left panel) and projected density of states (DOS) of C3 together with those of N-doped structures (right panel), namely N1, N2 and N3. The contour plots of charge density of selected states were shown in the left panel and the contour value is 0.05 a.u. The C atoms are in brown, the N atoms are in light blue and marked with "N". The selected atoms are marked "*" in the left panel.

The optimized structures and E_b s for the Pt atoms mono-dispersed on N3 are summarized and compared with those on pristine GN in Table 1. Due to the hexagonal symmetry of the N3 and GN, totally 7 deposition structures on N3 were considered (Table 1). They can be classified into 3 types according to the coordination of the Pt atom with the N3 support, namely the Atop sites where the Pt atom stands immediately on top of a C or N atom, the Brg site where the Pt atom stands in the middle of 2 nearest neighboring C or N atoms, and the Hol site where the Pt atom interacts with more than 2 neighboring C or N atoms. In the most plausible deposition structure, the Pt atom lies on the centre of the triangle formed by the 3 N atoms in N3. Due to the difference in size among Pt, C, and N atoms, Pt atoms cannot be embedded into the basal plane of GN. Instead, the Pt atom stands 1.75 Å above the lattice plane to relax the tension and gain additional stability. The corresponding E_b is calculated as -4.47 eV and is more than doubled as compared with that on pristine GN. The differential charge density showed that there are significant charge accumulation regions between the Pt atom and the 3 N atoms and the charge transfer from Pt atom to N3 support is only 0.20 |e|, implying the partially covalent nature of the interaction (Fig. 2).

Table 1. Optimized structures and energetics for Pt atomic deposition on GN.

Model	E_b^a (eV)	h^b (Å)	Min $R_{Pt-C/N}^c$ (Å)	Δq^d (e)
N3:				
Atop-N ^e				
Brg-CN ^e				
Atop-C ^f				
Brg-CC ^g	-1.92	2.21	2.06	0.14
Brg-CC ^h	-1.99	2.11	2.06	0.17
Hol-C5N ^e				
Hol-N3	-4.47	1.75	2.09	0.20
Pristine GN:				
Atop	-1.89	2.04	2.04	0.03
Brg	-2.03	1.98	2.10	0.09
Hol	-1.41	1.97	2.43	0.01

^a The binding energy of Pt atom onto N3 and PG, calculated from Equation 1.

^b The distance of Pt atom from the basal plane of graphene. ^c The minimum distance from the deposited Pt atom to C or N atom on graphene. ^d The amount of charge transfer from Pt atom to the graphenic support. ^e The Pt atom diffuses to Hol-N3 during the structure relaxation. ^f The Pt atom diffuses to the Brg-CC site nearest neighboring a N atom. ^g The Brg-CC site nearest neighboring a N atom. ^h The Brg-CC site second nearest neighboring a N atom.

One of the key challenges for implementation of monodispersed ultrafine TM NP catalysts is that, due to the weak binding with the support and the influence of the reaction environments, the low diffusion barriers of TM atoms make their aggregation and sintering facile.³³ The calculated barrier for Pt atomic diffusion from Brg to the nearest neighboring Atop on pristine GN is as low as ~0.14 eV.⁶⁸ This low diffusion barrier implies that the deposited Pt atoms are ready to diffuse on GN and will form large particles as the amount of deposited Pt atoms increases. As a result, GN is not eligible as a support

material to immobilize single Pt atom for catalytic applications. The large E_b of PtN3 makes the outward diffusion of Pt to its adjacent Brg site 2.55 eV endothermic. The calculated barrier for this diffusion is 2.97 eV and is much higher than the Pt atomic diffusion barrier (~0.14 eV) over GN, which makes the clustering of deposited Pt atoms on PtN3 hard to take place under conventional condition. As the pyridinic N doped NG has been used as support to disperse TM atoms and NPs recently, we will focus on PtN3 in the following discussion.⁴⁷ The formation energy of PtN3 was also calculated and compared with N-doped structures, to strengthen the discussion on the stability and possible formation. E_f of PtN3 is -12.08 eV and is -2.76 eV lower than that of N3, showing that the formation of PtN3 would be also spontaneous in existence of bulk Pt and N3, while N3 is one of the most stable pyridinic-N doped NG structures.

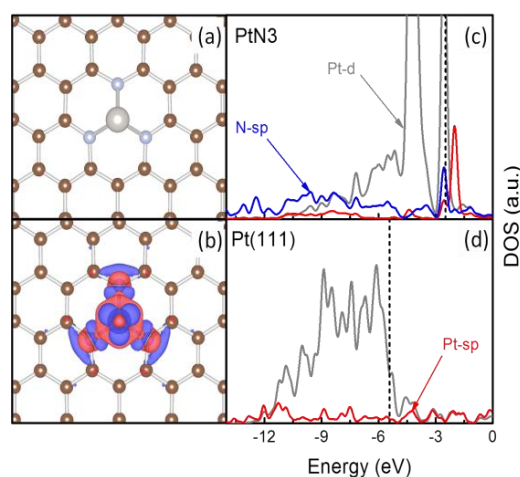


Fig. 2 Structure (a), contour plot of differential charge density (b) and DOS of PtN3 (c) compared with that of Pt(111) surface (d). (C: Brown; N: Light blue; Pt: Silver. The contour value of the differential charge density is ± 0.005 a.u. The charge accumulation regions are in red while the charge depletion regions are in blue. The DOS curves are aligned by the calculated vacuum level which is set as 0 and the E_F of each system is marked with the dashed lines.)

We compared the DOS of PtN3 and Pt(111) (Fig. 2) and noticed that not only the relative energy level of Pt-d states with respect to E_F but also the E_F of PtN3 are shifted up to the vacuum level. Those up-shifted Pt-d states resonance strongly with Pt-sp and N-sp states over a wide range from ~-10 eV to the E_F , showing that this up-shift is due to the interaction among these states. Accompanying the formation of this interfacial interaction, E_F of PtN3 is also up-shifted by 2.95 eV with respect to that of Pt(111) and some Pt-d states are standing right at the E_F , implying that the transfer of Pt-d electron from PtN3 for the activation of adsorbates would be much easier. The energy levels of localized d states of TMs are known to be vital for the activation of adsorbed reactants and subsequent reactions.²¹ The existence of these high energy Pt-d states and low workfunction originated from the interfacial Pt-N interaction suggest that PtN3 may exhibit superior reactivity in activation of adsorbed CO and O₂ for CO oxidation.

3.2 CO, O₂, O and CO₂ adsorption on PtN₃

We moved on to investigate the adsorption of O₂, CO, O and CO₂ which are possible reactants and products for the CO oxidation over PtN₃ (Table 2 and Fig. 3) to show the potential impact their adsorption on the reaction thermodynamics and kinetics. We noticed that CO, O₂ and CO₂ are only physisorbed, while O interacts moderately with pristine GN. The adsorption stabilities of all these species are significantly enhanced on PtN₃. The E_{ads} change from about -0.10 eV to -2.70, -1.89, -5.03 and -0.75 eV for CO, O₂, O and CO₂, respectively, indicating that all of them can be readily adsorbed onto the PtN₃ at low temperatures.

Table 2. The E_{ads} and the most plausible structures of various reaction species adsorption on PtN₃.

Species	E_{ads}^a (eV)	Bonding Details	
		Bond	Length (Å)
CO	-2.70	C-O	1.17
		Pt-C	1.85
O ₂	-1.89	O-O	1.38
		Pt-O	2.05
		Pt-O	2.05
O	-5.03	Pt-O	1.80
CO ₂	-0.75	Pt-O	2.34
		C-O	1.20
		C-O	1.24

^a The E_{ads} is calculated as the energy difference between the species adsorbed on PtN₃ and the gaseous species plus the bare PtN₃ according to equation 3.

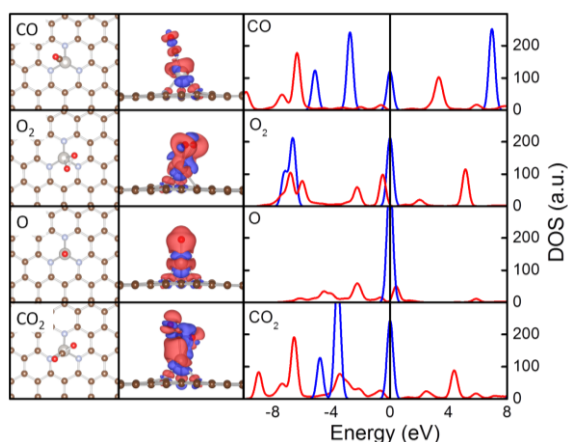


Fig. 3 The most plausible adsorption structures (left panel), contour plots of differential charge density (middle panel) and the corresponding DOS curves (right panel) for CO, O₂, O and CO₂ adsorption on PtN₃. (C: Brown; Pt: Silver; N: Light blue; O: Red. For the contour plots, the charge accumulation regions are rendered in red while the charge depletion regions are shown in blue. The contour value of the differential charge density is ± 0.005 a.u. The DOS curves of free species are in blue and those of adsorbed species are in red. The DOS curves are aligned by the calculated energy levels of highest occupied states of free species.)

In the most plausible CO adsorption configuration, the C-Pt distance is 1.85 Å and is typical in Pt containing metallorganic compounds. The strong hybridization of Pt with the support makes the impact of John-Teller distortion significant. As a result, the charged Pt atom prefer to interact with CO by forming the Pt-C bond in the direction of Pt- d_{z^2} state with a N-Pt-CO angle of 155.62°. ⁶⁹ Comparing with the free CO

molecule, the C-O distance was elongated from 1.14 Å in a free molecule to 1.17 Å after adsorption. To ease the charge transfer for activation, O₂ binds with PtN₃ along the direction of Pt- t_{2g} states, immediately on top of the deposited Pt atom with a nearest Pt-O distance of 2.05 Å. Adsorption in this way also elongates the O-O distance by about 0.2 Å with respect to gaseous O₂. As for the case of CO₂, the Pt atom stands immediately below one of the C-O bond and the nearest O-Pt and C-Pt distances are 2.13 Å and 2.05 Å, respectively, and CO₂ is significantly distorted: One of the C-O distance is elongated to 1.29 Å, the other C-O distance is 1.20 Å and the O-C-O angle is deformed from 180° to 142.06°. Previously, distortion of O-C-O angle at this level was only observed during CO₂ activation and adsorption over framework anions. ⁷⁰ The CO₂ activation adsorption over PtN₃ also shows the potential application of PtN₃ for CO₂ sequestration and conversion.

The adsorption of these reaction species is accompanied with charge transfer. It is apparent from Fig. 3 that the charge is always transferred from the Pt to the adsorbed molecules. The amount of charge transfer is 0.10, 0.28, and 0.42 |e| for CO, O₂ and O, respectively. The charge accumulation regions are localized between C-Pt and O-Pt and mainly on O for the adsorption of CO, O₂ and O, respectively, showing the partial covalent nature of newly formed C-Pt and O-Pt bonds. There are also charge depletion regions between C-O (for CO) and O-O (for O₂), showing the activation of CO and O₂ upon adsorption. The charge transfer between CO₂ and PtN₃ is similar to that of CO. Charge is accumulated between C-Pt and O-Pt and is depleted between C-O, suggesting the formation of Pt-C and Pt-O interaction and weakening of the C-O interaction.

The DOS analysis was performed to visualize the orbital interaction associated with the charge transfer. Due to the orbital interaction with the Pt-sp, Pt-d states, the states of adsorbates are all downshifted and some partially or unoccupied states even get occupied and downshifted to below E_F . After adsorption, the peak of CO- $2\pi^*$ state is split into parts due to the charge transfer from PtN₃ and even shifted to below E_F , suggesting the activation of CO and is accord with the elongation of C-O distance. The case for O₂ adsorption is similar to that of CO. The DOS peaks of O₂- 5σ and O₂- 2π states are downshifted, showing their strong hybridization and charge transfer with Pt-d and Pt-sp states. The existence of DOS peaks of O₂- 2π states below E_F indicates that O₂- 2π state gains charge from PtN₃ and O₂ is activated. As for O adsorption, the distribution of DOS curve of O-sp states is quite similar to those of adsorbed O₂, indicating the effectiveness of PtN₃ for O₂ activation. Due to the lack of repulsive interaction among negative charge absorbed O atoms, the adsorption of O is much stronger than that of O₂ and this phenomenon is widely observed in coverage dependent O adsorption on surfaces of transition metals and alloys. ^{71, 72} We also analyzed the interaction between CO₂ and PtN₃ and found that one of the π states of CO₂ interacts strongly the Pt states and is downshifted to right below E_F , showing the charge transfer from PtN₃ to this state and the activation of the corresponding C-O bond.

As both CO and O₂ interact strongly with PtN₃, one may concern the stability of PtN₃ in existence of CO or O₂. The adsorption of CO and O₂ on a Pt atom on a C=C bridge site nearest neighbouring a N atom (PtC2) was also investigated and the calculated total energies were directly compared with those over PtN₃ to deduce the thermodynamics for the possible adsorbates mediated diffusion of Pt atom. The adsorption structures of CO and O₂ over PtN₃ are more stable as compared with those over PtC2 and the differences in total energies are 1.28 and 1.71 eV for CO and O₂, respectively. This implies that the outward diffusion of Pt atom from N3 to C2 in existence of adsorbed CO and O₂ is still endothermic and the diffusion barriers would be more than the difference in total energies to overcome the endothermicity of the process. Furthermore, we also observed the inward diffusion of Pt atom with the help of adsorbed O₂ during the optimization. These results suggest that PtN₃ is stable in reaction environment.

It should be noted that, according to the calculated E_{ads}, the adsorption of CO on PtN₃ is preferred rather than O₂, but the coadsorption of CO together with an O₂ is still exothermic and the E_{ad} (-3.16 eV) is even larger than the adsorption of only a CO or an O₂. Due to the charge accumulation on CO and depletion on PtN₃, the coadsorption of 2 CO is thermodynamically less preferred by 0.35 eV as compared with the coadsorption of CO and O₂. This suggests that PtN₃ is hard to be poisoned by CO.

3.3 CO oxidation over PtN₃

As a heterogeneous reaction, CO oxidation may proceed through either the Langmuir-Hinshelwood (LH) mechanism or the Eley-Rideal (ER) mechanism, depending on the chemical nature of the catalysts.⁷³ The CO oxidation following LH mechanism starts with the interaction between the coadsorbed CO and O₂ molecules for formation of a peroxide-like O=C-O-O intermediate. As the coadsorbed CO and O₂ are all negatively charged and repulsive to each other, the formation of the peroxide becomes demanding and sets the rate of the process. Different from the LH mechanism, the ER mechanism doesn't require the coadsorption of both CO and O₂ and is the common mechanism for CO oxidation over catalysts that are ready for the activation of O₂. In O-rich environment, the CO oxidation following ER mechanism initiates with the direct reaction of gaseous CO molecules with the activated O₂ at the reaction centers to form a carbonate-like CO₃ intermediate. As the CO is not activated and the CO₃ intermediate is always too stable, the reaction rate may be determined by either the formation or the dissociation of CO₃.⁴⁹ To investigate the thermodynamics of the CO oxidation over PtN₃ through both mechanisms, the total energy of all possible states along the reaction paths were aligned by the sum of total energy of free gaseous CO and O₂ and clean PtN₃. The reaction of CO with O₂ over PtN₃ through both the ER and LH mechanisms was investigated.

We were considering the possible reaction between the preadsorbed O₂ and gaseous CO due to the fact that O₂ is highly activated, which may kinetically compete with the reaction between coadsorbed CO and O₂ over PtN₃. The relaxed

structures of various states along the reaction path following the ER mechanism were shown in Fig. 4. The physisorption of CO over preadsorbed O₂ on the PtN₃ was set as the initial state (ER-IS), as formation of the carbonate like intermediate (ER-MS1) requires direct reaction between the gaseous CO and the adsorbed O₂. After relaxation, the CO lies in plane with the adsorbed O₂ with the C-O direction vertical to that of O-O and the distance between the CO and 2 atoms of the adsorbed O₂ are both 3.67 Å in ER-IS. When new C-O interactions between the CO and the activated O₂ become mature, ER-MS1 is formed. In ER-MS1, the O-O distance is 2.20 Å which is enlarged by 0.82 Å as compared that in adsorbed O₂. Similar carbonate intermediate structures have been found in the CO oxidation over Fe atoms embedded in graphene and supported Au nanoparticles.^{9, 49, 74} As a net effect of generation of new C-O bonds and scission of the O-O bond, the formation of ER-MS1 is exothermic by 3.03 eV with respect to ER-IS and requires crossing a barrier of 0.89 eV (ER-TS1). Further dissociation of ER-MS1 forms a CO₂ and an adsorbed O atom (ER-MS2) by breaking one of the C-O bonds connected to PtN₃. As the ER-MS1 is relatively stable and the adsorbed single O atom is highly reactive, the reaction along this path is endothermic by 0.93 eV with respect to ER-MS1 and requires crossing of another high energy barrier of 1.41 eV (ER-TS2). The barriers for formation of ER-MS1 and ER-MS2 are all more than 0.8 eV, implying that the CO oxidation over PtN₃ through ER mechanism would be hindered by these high reaction barriers, especially the dissociation of ER-MS1.

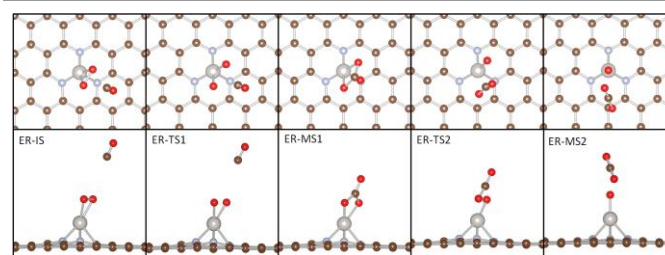


Fig. 4 Top views (Top panel) and side views (Bottom panel) of local configurations of the adsorbates on the PtN₃ at various states along the minimum-energy pathway via the ER mechanism, including the initial state (ER-IS), transition state (ER-TS1 and ER-TS2), intermediate state (ER-MS1) and final state (ER-MS2). (C: Brown; O: Red; N: Light blue; Pt: Silver.)

Though the John-Teller effect is significant due to the interaction between Pt atom and the N₃ support, the Pt atom is still not fully coordinated in a distorted octahedron even in the adsorption structures of CO and O₂. This suggests that the coadsorption of CO and O₂ may be more favorable than the solo adsorption of O₂ and can serve as the initial point for the CO oxidation. As expected, the coadsorption of CO and O₂ over PtN₃ (LH-IS1) is found 1.23 eV more stable as compared with ER-IS. The previous investigations on the CO oxidation over Au and Cu atoms embedded in graphene suggested that LH mechanism would be thermodynamically more favorable than the ER mechanism.^{48, 50} Therefore, we moved on to investigate CO oxidation through the LH mechanism.

Table 3. Structural Parameters for Various States along the MEP for the CO Oxidation over PtN3 through LH mechanism.

States	d_{C-O}^a (Å)	d_{C-Pt}^a (Å)	d_{C-O1}^a (Å)	d_{C-O2}^a (Å)	d_{O1-O2}^a (Å)	d_{O1-Pt}^a (Å)	d_{O2-Pt}^a (Å)	\angle_{O-C-O1}^b (°)	\angle_{O-C-O2}^b (°)
LH-IS1	1.16	1.89	2.13	--	1.30	2.91	--	131.59	--
LH-TS1	1.15	1.90	2.98	--	1.30	2.09	--	109.54	--
LH-MS1	1.21	2.00	1.38	--	1.50	2.06	--	121.64	--
LH-TS2	1.22	2.05	1.33	--	1.73	1.97	--	123.91	--
LH-MS2	1.17	4.13	1.17	--	3.38	1.81	--	178.76	--
LH-IS2	1.14	3.83	--	3.11	--	--	1.81	--	97.88
LH-TS3	1.15	2.69	--	2.78	--	--	1.85	--	94.44
LH-FS	1.20	2.05	--	1.29	--	--	2.13	--	142.06

^a The distance between specific atoms as nominated in Fig. 5. ^b The angle among O-C-O. This angle is 120° in CO₃²⁻ and is 180° in free CO₂.

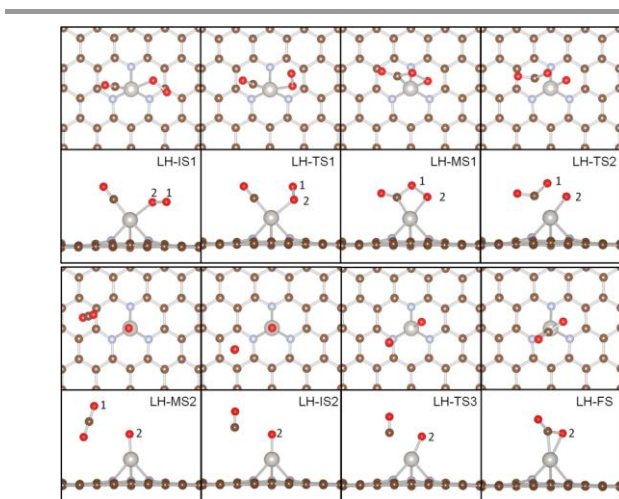


Fig. 5. Top views (Top panel) and side views (Bottom panel) of local configurations of the adsorbates on the PtN3 at various states along the MEP via the LH mechanism, including the initial states (LH-IS1 and LH-IS2), transition states (LH-TS1, LH-TS2 and LH-TS3), intermediate states (LH-MS1 and LH-MS2) and the final state (LH-FS). (C: Brown; N: Light Blue; O: Red; Pt: Silver.)

The most plausible coadsorption structures of CO and O₂, together with the atomic structures at various states along the MEP following the LH mechanism are shown in Fig. 5 and the structural parameters are listed in Table 3. As CO and O₂ all gains charge from the anchored Pt atom, they are repulsive to each other and this repulsive interaction makes the coadsorption structure unstable by 1.43 eV with respect to the separate adsorption of CO and O₂. Resulting from this, the O1-O2 distance decreases to 1.30 Å and the C-Pt distance increases from 1.85 Å to 1.89 Å in LH-IS1. The interaction between CO and O₂ initiates after their coadsorption, with the connecting of the O atom (O1) in the adsorbed O₂ to CO to form the transition state (LH-TS1) that links LH-IS1 to LH-MS1. The decrease of the C-O1 distance between CO and O₂ that are repulsive to each other from 2.91 Å in LH-IS1 to 2.09 Å in LH-TS1 makes this journey endothermic by 0.01 eV with respect to LH-IS1. The formation of the peroxide-like O2-O1-C-O complex (LH-MS1) is only exothermic by 0.07 eV as compared with LH-IS1. Accompanying the formation of C-O1 bond, the O1-O2 distance is further elongated from 1.30 Å to 1.50 Å. The O-O

distance at this length scale has been only be observed in peroxide before, suggesting the instability of LH-MS1 and the easiness for the scission of the O1-O2 bond. An adsorbed O atom and a physisorbed CO₂ (LH-MS2) will be formed by the scission of the elongated O-O bond in LH-MS1. As a joint effect of the generation of C=O bonds and the scission of elongated O-O and Pt-C bonds, the formation of LH-MS2 is exothermic by 1.81 eV with respect to LH-MS1 and requires crossing LH-TS2 with an energy barrier of 0.07 eV. The small barrier suggests that decomposition of LH-MS1 is a spontaneous process and is ready to take place at low temperatures. In the corresponding TS (LH-TS2), the O-O distance is further enlarged to 1.73 Å, the Pt-C distance is enlarged from 2.00 Å in LH-MS1 to 2.05 Å, while the C-O1 distance is shortened from 1.38 Å to 1.33 Å, indicating the strengthening of the C-O1 interaction and the weakening of the O1-O2 and Pt-C interaction taking place simultaneously. As a result, the C(CO₂)-Pt and C(CO₂)-O2 distances are further enlarged to 4.13 and 3.16 Å in LH-MS2, respectively, and the desorption of CO₂ can also be considered to be barrierless. Comparing with MEP for CO oxidation through ER mechanism, LH-IS1 is more stable and the reaction barriers for formation and dissociation of LH-MS1 are much smaller, showing the superiority of LH mechanism for CO oxidation.

The subsequent reaction takes place between a gaseous CO molecule and the adsorbed O atom over PtN3. As the desorption of the CO₂ from LH-MS2 is barrierless, the initial state was set as a configuration in which a gaseous CO is more than 3.0 Å from the remnant O on PtN3 (LH-IS2). The product was set to the configuration that CO₂ adsorbed on PtN3 (LH-FS). The reaction initiates with the approaching of the C atom in CO to the remnant O to reach the transition state (LH-TS3). Within LH-TS3, the Pt-C(CO) distance is decreased from 3.83 Å in LH-IS2 to 2.69 Å and the C-O2 distance is also decreased from 3.11 to 2.78 Å, showing that due to the formation of interaction between CO and preadsorbed O atom, the CO molecule is pulled to PtN3 in this endothermic process. As expected from the high reactivity of the adsorbed O atom and the strong exothermic formation of CO₂, the formation of LH-FS is exothermic by 1.93 eV with respect to LH-IS2 and the corresponding reaction barrier is 0.15 eV.

One may consider the enhanced adsorption of CO_2 would hinder the subsequent adsorption and reaction of CO and O_2 . We tried to locate the coadsorption structures of CO or O_2 with CO_2 , but found in both cases CO_2 gets desorbed from PtN3 during the structural relaxation. This implies that though the CO_2 adsorption is enhanced but its desorption would still be facile with the subsequent adsorption of CO or O_2 . The statement is further enhanced when we take into consideration the stronger adsorption of CO and O_2 as compared with CO_2 , and the significant exothermicity for CO_2 formation. The low barrier for formation and desorption of CO_2 indicates that the regeneration of PtN3 as the available reaction center for subsequent CO oxidation is facile.

We also investigated the possibility for CO reaction with oxidized graphene. The calculated energy barrier for O_2 activated adsorption for formation of 2 adsorbed O atoms on pristine graphene is at the level of 3.0 eV. This high reaction barrier suggests that PG oxidation is not likely to take place in conventional reaction condition. We then moved on to consider the thermodynamics of the spillover of activated O atom from PtN3 to graphene and found that only O atom attached to PtN3 in the O_2 adsorption configuration is stable. The diffusion of one O atom of O_2 to the graphene region will destabilize the system by at least 1.1 eV, so the O atomic diffusion barrier would be more than 1.1 eV. In this sense, the oxidation of NG with O atoms from O_2 activated at PtN3 is still hard to take place. Therefore, PtN3 would be the dominant reaction center for the CO oxidation. The thermodynamics profile for CO oxidation over PtN3 is schematically summarized in Fig. 6.

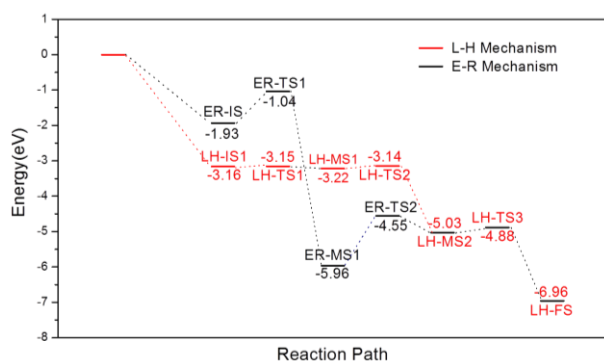


Fig. 6. Schematic energy profile corresponding to local configurations shown in Fig. 4 and 5 along the MEP for CO oxidation over PtN3. All energies are given with respect to the reference energy, i.e., the sum of energies of the clean PtN3 and gaseous CO and O_2 molecules.

In summary, the CO oxidation over PtN3 may be explained as a two-step process: The reaction cycle is initiated through the LH mechanism, where the coadsorbed CO and O_2 (LH-IS1) react to form a peroxide like complex (LH-MS1), by the dissociation of which the a CO_2 molecule and an adsorbed O atom are formed (LH-MS2), and then the PtN3 is regenerated to be available by the reaction of a gaseous CO with the adsorbed O atom (LH-IS2) to form another CO_2 (LH-FS). We investigated the evolution of DOS of O_2 and CO states during the reaction (SI information) and realized that the potential high catalytic

performance of PtN3 can be attributed to the compatibility of the states of PtN3 and adsorbed intermediates, particularly among the Pt-d states and the molecular states of CO and O_2 , that facilitates the required charge transfer for the reaction to proceed. The enhancement of the adsorption of CO , O_2 and CO_2 and the stability of intermediates that is nearly proportional to the up-shift of Pt-d states also vigorously visualizes this promotion effect resulting from the interfacial Pt-N interaction.⁷⁵

Conclusions

We investigated the electronic structure and the catalytic performance in CO oxidation of Pt atoms monodispersed on NG by first-principles-based calculations. We showed that the N-doping can introduce localized defect states to the vicinal at the E_F of GN, which will effectively stabilize the deposited Pt atoms. The binding of a single Pt atom onto N3 is up to -4.47 eV, which makes the sintering and aggregation of anchored Pt atoms at N3 not likely to take place. Both the calculated reaction thermodynamics and kinetics suggest that CO oxidation over PtN3 would proceed through the Langmuir–Hinshelwood mechanism. The calculated energy barriers for the formation and dissociation of peroxide-like intermediate are as low as 0.01 and 0.08 eV, respectively, while that for the regeneration of the anchored Pt atom is only 0.15 eV, indicating the potential high catalytic performance of PtN3 for low temperature CO oxidation. The Pt-d state that is upshifted to stand on the E_F and the low workfunction originated from the interfacial Pt-N interaction account for the enhanced activation of O_2 and the efficient formation and dissociation of peroxide-like intermediate. These findings suggest that controlled doping of the support material can introduce defect states that can significantly impact the electronic structure of deposited TM atoms or NPs to achieve a superior catalytic performance, and call for the development of effective chemical routines that can fabricate doped graphene in a well-defined way.

Author Contributions

X. L. designed the research and wrote the manuscript. Y. S. conceived the calculations and analyzed the results. Y. S. is responsible for the calculation results. Y. H. and C. G. M. proofed the manuscript and polished the language. All authors have given approval to the final version of the manuscript.

Acknowledgements

This work was supported by NSFC (21373036, 21103015, and 21271037), the Fundamental Research Funds for the Central Universities (DUT12LK14 and DUT14LK09), the Key Laboratory of Coastal Zone Environmental Processes YICCAS (201203), the Key Science and Technology International Cooperation Foundation of Hainan Province, China (KJHZ2014-08) and the Special Academic Partner GCR Program from King Abdullah University of Science and Technology. Y. H would also thank Dalian University of Technology for the Seasky Professorship.

Notes and references

^a School of Chemistry, Dalian University of Technology, Dalian, 116024, P. R. China. Email: xliu@dlut.edu.cn.

^b Advanced Membranes and Porous Materials Center, King Abdullah University of Science and Technology, Thuwal, 23955-6900, Kingdom of Saudi Arabia.

† Electronic Supplementary Information (ESI) available: Evolution of CO and O₂ DOS during the reaction. See DOI: 10.1039/b000000x/

1. A. Alavi, P. J. Hu, T. Deutsch, P. L. Silvestrelli and J. Hutter, *Phys. Rev. Lett.*, 1998, **80**, 3650-3653.
2. W. T. Yu, M. D. Porosoff and J. G. G. Chen, *Chem. Rev.*, 2012, **112**, 5780-5817.
3. R. Siburian, T. Kondo and J. Nakamura, *J. Phys. Chem. C*, 2013, **117**, 3635-3645.
4. S. Shan, V. Petkov, L. Yang, J. Luo, P. Joseph, D. Mayzel, B. Prasai, L. Wang, M. Engelhard and C.-J. Zhong, *J. Am. Chem. Soc.*, 2014, **136**, 7140-7151.
5. R. Toyoshima, M. Yoshida, Y. Monya, Y. Kousa, K. Suzuki, H. Abe, B. S. Mun, K. Mase, K. Amemiya and H. Kondoh, *J. Phys. Chem. C*, 2012, **116**, 18691-18697.
6. Z. P. Liu and P. Hu, *J. Chem. Phys.*, 2001, **115**, 4977-4980.
7. A. Eichler, *Surf. Sci.*, 2002, **498**, 314-320.
8. M. S. Chen, Y. Cal, Z. Yan, K. K. Gath, S. Axnanda and D. W. Goodman, *Surf. Sci.*, 2007, **601**, 5326-5331.
9. Z.-P. Liu, P. Hu and A. Alavi, *J. Am. Chem. Soc.*, 2002, **124**, 14770-14779.
10. N. Lopez and J. K. Nørskov, *J. Am. Chem. Soc.*, 2002, **124**, 11262-11263.
11. M. L. Kimble, A. W. Castleman, R. Mitric, C. Burgel and V. Bonacic-Koutecky, *J. Am. Chem. Soc.*, 2004, **126**, 2526-2535.
12. S. H. Oh and G. B. Hoflund, *J. Catal.*, 2007, **245**, 35-44.
13. Q. Fu, W. X. Li, Y. X. Yao, H. Y. Liu, H. Y. Su, D. Ma, X. K. Gu, L. M. Chen, Z. Wang, H. Zhang, B. Wang and X. H. Bao, *Science*, 2010, **328**, 1141-1144.
14. J. Lin, B. T. Qiao, J. Y. Liu, Y. Q. Huang, A. Q. Wang, L. Li, W. S. Zhang, L. F. Allard, X. D. Wang and T. Zhang, *Angew. Chem.-Int. Edit.*, 2012, **51**, 2920-2924.
15. B. T. Qiao, A. Q. Wang, X. F. Yang, L. F. Allard, Z. Jiang, Y. T. Cui, J. Y. Liu, J. Li and T. Zhang, *Nat. Chem.*, 2011, **3**, 634-641.
16. H. A. Gasteiger, S. S. Kocha, B. Sompalli and F. T. Wagner, *Appl. Catal. B-Environ.*, 2005, **56**, 9-35.
17. J. Lin, A. Wang, B. Qiao, X. Liu, X. Yang, X. Wang, J. Liang, J. Li, J. Liu and T. Zhang, *J. Am. Chem. Soc.*, 2013, **135**, 15314-15317.
18. M. Moses-DeBusk, M. Yoon, L. F. Allard, D. R. Mullins, Z. Wu, X. Yang, G. Veith, G. M. Stocks and C. K. Narula, *J. Am. Chem. Soc.*, 2013, **135**, 12634-12645.
19. J. Z. Zhang, X. Liu, M. N. Hedhili, Y. H. Zhu and Y. Han, *ChemCatChem*, 2011, **3**, 1294-1298.
20. X. F. Yang, A. Q. Wang, B. T. Qiao, J. Li, J. Y. Liu and T. Zhang, *Accounts of Chemical Research*, 2013, **46**, 1740-1748.
21. B. Hammer and J. K. Nørskov, in *Advances in Catalysis*, Academic Press Inc, San Diego, 2000, pp. 71-129.
22. I. N. Remediakis, N. Lopez and J. K. Nørskov, *Angew. Chem.-Int. Edit.*, 2005, **44**, 1824-1826.
23. X. Liu, S. B. Zhang, X. C. Ma, J. F. Jia, Q. K. Xue, X. H. Bao and W. X. Li, *Appl. Phys. Lett.*, 2008, **93**, 093105.
24. L. Li, A. H. Larsen, N. A. Romero, V. A. Morozov, C. Glinsvad, F. Abild-Pedersen, J. Greeley, K. W. Jacobsen and J. K. Nørskov, *J. Phys. Chem. Lett.*, 2013, **4**, 222-226.
25. X. Liu, Y. Sui, C. Meng and Y. Han, *RSC Adv.*, 2014, **4**, 22230-22240.
26. X. Liu, C. Meng and Y. Han, *Nanoscale*, 2012, **4**, 2288-2295.
27. X. Liu, K. X. Yao, C. Meng and Y. Han, *Dalton Trans.*, 2012, **41**, 1289-1296.
28. X. Liu, L. Li, C. Meng and Y. Han, *J. Phys. Chem. C*, 2012, **116**, 2710-2719.
29. K. X. Yao, X. Liu, Z. Li, C. C. Li, H. C. Zeng and Y. Han, *ChemCatChem*, 2012, **4**, 1938-1942.
30. M. S. Chen and D. W. Goodman, *Chem. Soc. Rev.*, 2008, **37**, 1860-1870.
31. Y. X. Yao, X. Liu, Q. Fu, W. X. Li, D. L. Tan and X. H. Bao, *ChemPhysChem*, 2008, **9**, 975-979.
32. A. Uzun, V. Ortalan, Y. L. Hao, N. D. Browning and B. C. Gates, *ACS Nano*, 2009, **3**, 3691-3695.
33. A. Uzun, V. Ortalan, N. D. Browning and B. C. Gates, *J. Catal.*, 2010, **269**, 318-328.
34. A. A. Herzing, C. J. Kiely, A. F. Carley, P. Landon and G. J. Hutchings, *Science*, 2008, **321**, 1331-1335.
35. W. C. Ding, X. K. Gu, H. Y. Su and W. X. Li, *J. Phys. Chem. C*, 2014, **118**, 12216-12223.
36. P. P. Hu, Z. W. Huang, Z. Amghouz, M. Makkee, F. Xu, F. Kapteijn, A. Dikhtiarenko, Y. X. Chen, X. Gu and X. F. Tang, *Angew. Chem.-Int. Edit.*, 2014, **53**, 3418-3421.
37. S. Sun, G. Zhang, N. Gauquelin, N. Chen, J. Zhou, S. Yang, W. Chen, X. Meng, D. Geng, M. N. Banis, R. Li, S. Ye, S. Knights, G. A. Botton, T.-K. Sham and X. Sun, *Sci. Rep.*, 2013, **3**, 1775.
38. A. K. Geim, *Science*, 2009, **324**, 1530-1534.
39. D. W. Wang and D. S. Su, *Energy Environ. Sci.*, 2014, **7**, 576-591.
40. L. P. Zhang and Z. H. Xia, *J. Phys. Chem. C*, 2011, **115**, 11170-11176.
41. Y. Zheng, Y. Jiao, Y. H. Zhu, L. H. Li, Y. Han, Y. Chen, A. J. Du, M. Jaroniec and S. Z. Qiao, *Nat. Commun.*, 2014, **5**, 3783.
42. L. M. Dai, *Accounts of Chemical Research*, 2013, **46**, 31-42.
43. T. Xing, Y. Zheng, L. H. Li, B. C. C. Cowie, D. Gunzelmann, S. Z. Qiao, S. Huang and Y. Chen, *ACS Nano*, 2014, **8**, 6856-6862.
44. L. S. Zhang, X. Q. Liang, W. G. Song and Z. Y. Wu, *Phys. Chem. Chem. Phys.*, 2010, **12**, 12055-12059.
45. R. I. Jafri, N. Rajalakshmi and S. Ramaprabhu, *J. Mater. Chem.*, 2010, **20**, 7114-7117.
46. T. Kondo, T. Suzuki and J. Nakamura, *J. Phys. Chem. Lett.*, 2011, **2**, 577-580.
47. B. Xiong, Y. Zhou, Y. Zhao, J. Wang, X. Chen, R. O'Hayre and Z. Shao, *Carbon*, 2013, **52**, 181-192.
48. Y. H. Lu, M. Zhou, C. Zhang and Y. P. Feng, *J. Phys. Chem. C*, 2009, **113**, 20156-20160.
49. Y. Li, Z. Zhou, G. Yu, W. Chen and Z. Chen, *J. Phys. Chem. C*, 2010, **114**, 6250-6254.
50. E. H. Song, Z. Wen and Q. Jiang, *J. Phys. Chem. C*, 2011, **115**, 3678-3683.

51. Y. N. Tang, Z. X. Yang, X. Q. Dai, D. W. Ma and Z. M. Fu, *J. Phys. Chem. C*, 2013, **117**, 5258-5268.
52. B. Delley, *Phys. Rev. B*, 2002, **66**, 155125.
53. B. Delley, *J. Chem. Phys.*, 1990, **92**, 508-517.
54. B. Delley, *J. Chem. Phys.*, 2000, **113**, 7756-7764.
55. J. P. Perdew, K. Burke and M. Ernzerhof, *Phys. Rev. Lett.*, 1996, **77**, 3865-3868.
56. X. Liu, C. G. Meng and C. H. Liu, *Phase Transit.*, 2006, **79**, 249-259.
57. X. Liu, C. G. Meng and C. H. Liu, *Acta Phys.-Chim. Sin.*, 2004, **20**, 280-284.
58. N. Govind, M. Petersen, G. Fitzgerald, D. King-Smith and J. Andzelm, *Comput. Mater. Sci.*, 2003, **28**, 250-258.
59. H. J. Monkhorst and J. D. Pack, *Phys. Rev. B*, 1976, **13**, 5188-5192.
60. F. L. Hirshfeld, *Theor. Chim. Acta*, 1977, **44**, 129-138.
61. H. T. Liu, Y. Q. Liu and D. B. Zhu, *J. Mater. Chem.*, 2011, **21**, 3335-3345.
62. X. Wang, Y. Liu, D. Zhu, L. Zhang, H. Ma, N. Yao and B. Zhang, *J. Phys. Chem. B*, 2002, **106**, 2186-2190.
63. Z. Q. Luo, S. H. Lim, Z. Q. Tian, J. Z. Shang, L. F. Lai, B. MacDonald, C. Fu, Z. X. Shen, T. Yu and J. Y. Lin, *J. Mater. Chem.*, 2011, **21**, 8038-8044.
64. Z. H. Sheng, L. Shao, J. J. Chen, W. J. Bao, F. B. Wang and X. H. Xia, *ACS Nano*, 2011, **5**, 4350-4358.
65. J. Kotakoski, A. V. Krasheninnikov, U. Kaiser and J. C. Meyer, *Phys. Rev. Lett.*, 2011, **106**, 105505.
66. D. W. Boukhvalov and M. I. Katsnelson, *Nano Lett.*, 2008, **8**, 4373-4379.
67. P. A. Denis and F. Iribarne, *J. Phys. Chem. C*, 2013, **117**, 19048-19055.
68. P. Blonski and J. Hafner, *J. Chem. Phys.*, 2011, **134**.
69. X. Liu, T. Duan, Y. Sui, C. Meng and Y. Han, *RSC Adv.*, 2014, **4**, 38750-38760.
70. Y. Zhao, X. Liu, K. X. Yao, L. Zhao and Y. Han, *Chem. Mat.*, 2012, **24**, 4725-4734.
71. W. X. Li, C. Stampfl and M. Scheffler, *Phys. Rev. B*, 2002, **65**, 075407.
72. X. Liu, H. Guo and C. Meng, *J. Phys. Chem. C*, 2012, **116**, 21771-21779.
73. K. J. Laidler, *Pure Appl. Chem.*, 1996, **68**, 149-192.
74. C. Liu, Y. Tan, S. Lin, H. Li, X. Wu, L. Li, Y. Pei and X. C. Zeng, *J. Am. Chem. Soc.*, 2013, **135**, 2583-2595.
75. W. An, Y. Pei and X. C. Zeng, *Nano Lett.*, 2008, **8**, 195-202.